Article

Theoretical Studies on the Mechanism of Inhibition of Ribonucleotide Reductase by (*E*)-2'-Fluoromethylene-2'-deoxycitidine-5'-diphosphate

Pedro Alexandrino Fernandes, and Maria Joo Ramos

J. Am. Chem. Soc., **2003**, 125 (20), 6311-6322• DOI: 10.1021/ja0208613 • Publication Date (Web): 24 April 2003

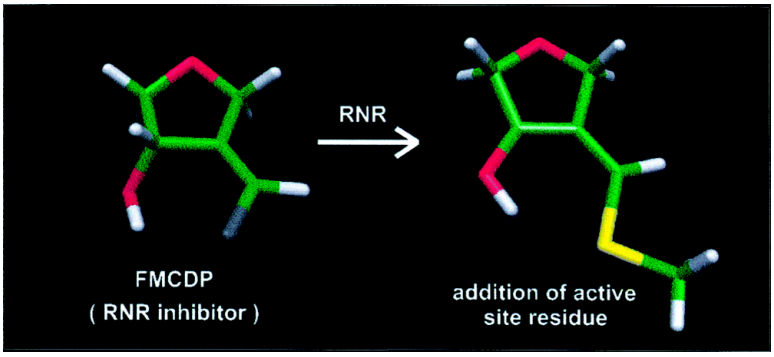

More About This Article

Additional resources and features associated with this article are available within the HTML version:

- Supporting Information
- Links to the 9 articles that cite this article, as of the time of this article download
- Access to high resolution figures
- Links to articles and content related to this article
- Copyright permission to reproduce figures and/or text from this article

View the Full Text HTML

J|A|C|S
ARTICLES
Published on Web 04/24/2003

Theoretical Studies on the Mechanism of Inhibition of Ribonucleotide Reductase by (*E*)-2′-Fluoromethylene-2′-deoxycitidine-5′-diphosphate

Pedro Alexandrino Fernandes and Maria João Ramos*

Contribution from the CEQUP/ Faculdade de Ciências do Porto, Rua do Campo Alegre, 687, 4169-007 Porto, Portugal

Received June 20, 2002; Revised Manuscript Received October 17, 2002; E-mail: mjramos@fc.up.pt

Abstract: (*E*)-2′-Fluoromethylene-2′-deoxycitidine-5′-diphosphate (FMCDP) is a potent time-dependent inactivator of the enzyme Ribonucleotide Reductase, which operates by destructing an essential tyrosil radical and performing a covalent addition to an active site residue. Considerable effort to elucidate the inhibition mechanism has been undertaken in recent years, and some insights have been obtained. Although a mechanistic proposal has been put forward, based on a general paradigm of inhibition of RNR by 2′ substituted substrate analogues, details about the mechanism have remained elusive. Namely, the exact residue that adds to the inhibitor is still not identified, although mutagenesis experiments suggest that it should correspond to the E441 residue. In this work, we performed an extensive theoretical exploration of the potential energy surface of a model system representing the active site of RNR with FMCDP, using Density Functional Theory. This study establishes the detailed mechanism of inhibition, which is considerably different from the one proposed earlier. The proposed mechanism is fully consistent with available experimental data. Energetic results reveal unambiguously that the residue adding to the inhibitor is a cysteine, most probably C439, and exclude the possibility of the addition of E441. However, the E441 residue is shown to be essential for inhibition, catalyzing both the major and minor inhibition pathways, in agreement with mutagenesis results. It is shown also that the major mode of inactivation mimics the early stages of the natural substrate pathway.

I. Introduction

Ribonucleotide Reductases (RNRs) are very important enzymes present in all living organisms. They catalyze the reduction of ribonucleotides to 2′-deoxyribonucleotides, the rate-limiting step in DNA replication and repair.[1−6] Therefore, they play a fundamental role in the regulation of cell growth, and have recently become a promising target for the design of new chemical therapeutic agents, mainly in the field of antitumor and antiviral treatments.[5,7−10] Recent in vivo experiments on the inactivation of the enzyme have revealed potent antiproliferative effects against a wide range of tumor cell lines,[10−12] as well as human xenografts in mice.[10,13−14] There are four classes of RNRs, according to the required cofactors necessary for catalytic activity. It is presently known that all of them follow a radical mechanism to dehydrate the substrate. Class I RNRs possess a stable tyrosil radical adjacent to a diiron cluster.[15,16] Class II RNRs use AdoCbl as cofactor.[17,18] Class III RNRs are expressed in anaerobic environment and possess a glycyl radical generated by an FeS cluster.[19,20] Class IV (presently suggested to be included in the Ib class) possesses a protein radical (probably a tyrosil radical) generated by a dimanganese cluster.[21−23] This study is devoted to Class I RNRs. The *E. Coli* ribonucleotide diphosphate reductase has been extensively investigated and serves as the prototype for the mammalian

(1) Stubbe, J.; van der Donk, W. A. *Chem. Rev.* **1998**, *98*, 705.
(2) Eriksson, S.; Sjöberg, B.-M. In *Allosteric Enzymes*; Hervé, G., Ed.; CRC: Boca Raton, 1989, p 189.
(3) Stubbe, J. *Adv. Enzymol. Relat. Areas Mol. Biol.* **1990**, *63*, 349.
(4) Reichard, P., *Science* **1993**, *260*, 1773−1777.
(5) Stubbe, J.; van der Donk, W. A. *Chem. Biol.* **1995**, *2*, 793.
(6) Sjöberg, B.-M. In *Nucleic Acids and Molecular Biology*; Eckstein, F., Lilley, D., Eds.; Springer: Berlin, 1995; Vol. 9, p 192.
(7) Cory, J. G.; Chiba, P. In *Combination Chemotherapy Directed at the Components of Nucleoside Diphosphate Reductase*; Cory, J. G., Cory, A. H., Eds.; Pergamon Press: New York, 1989; p 245.
(8) Robins, M. J.; Samano, M. C.; Samano, V. *Nucleosides Nucleotides* **1995**, *14*, 485.
(9) Nocentini, J. *Crit. Rev. Oncol. Hematol.* **1996**, *22*, 89.
(10) Gerfen, G. J.; van der Donk, W. A.; Yu, G.; McCarthy, J. R.; Jarvi, E. T.; Matthews, D. P.; Farrar, C.; Griffin, R. G.; Stubbe, J. *J. Am. Chem. Soc.* **1998**, *120*, 3823.
(11) McCarthy, J. R.; Sunkara, P. S. *Design, Synthesis and Antitumor Activity of an Inhibitor of Ribonucleotide Reductase*; Weiner, D. B., Williams, W. B., Eds.; CRC Press: Boca Raton, FL, 1995; pp 3−32.
(12) McCarthy, J. R.; Sunkara, P. S.; Matthews, D. P.; Bitonti, A. J.; Jarvi, E. T.; Sabol, J. S., Resvick, R. J.; Hubber, E. W.; van der Donk, W. A.; Yu, G.; Stubbe, J. *ACS Symp. Ser.* **1996**, *639*, 246.
(13) Bitonti, A. J.; Dumont, J. A.; Bush, T. L.; Cashman, E. A.; Crossdoersen, D. E., Wright, P. S.; Matthews, D. P.; McCarthy, J. R.; Kaplan, D. A. *Cancer Res.* **1994**, *54*, 1485.
(14) Bitonti, A. J.; Bush, T. L.; Lewis, M. T.; Sunkara, P. S. *Anticancer Res.* **1995**, *15*, 1179.
(15) Hammersten, E.; Reichard, P.; Saluste, E. *J. Biol. Chem.* **1950**, *183*, 105.
(16) Reichard, P.; Estborn, B. *J. Biol. Chem.* **1951**, *188*, 839.
(17) Blackley, R. L.; Barker, H. A. *Biochem. Byophys. Res. Commun.* **1964**, *16*, 391.
(18) Beck, H. S.; Hardy, J. *Proc. Natl. Acad. Sci. U.S.A.* **1965**, *54*, 286.
(19) Barlow, T. *Biochem. Byophys. Res. Commun.* **1988**, *155*, 747.
(20) Fontecave, M.; Eliasson, R.; Reichard, P. *Proc. Natl. Acad. Sci. U.S.A.* **1989**, *86*, 2147.
(21) Schimpff-Weiland, G.; Follman, H.; Auling, G. *Biochem. Byophys. Res. Commun.* **1981**, *102*, 1276.
(22) Willing, A.; Follman, H.; Auling, G. *Eur. J. Biochem.* **1988**, 178, 603.
(23) Griepenburg, U.; Lassman, G.; Auling, G. *Free Rad. Res.* **1996**, *26*, 473.

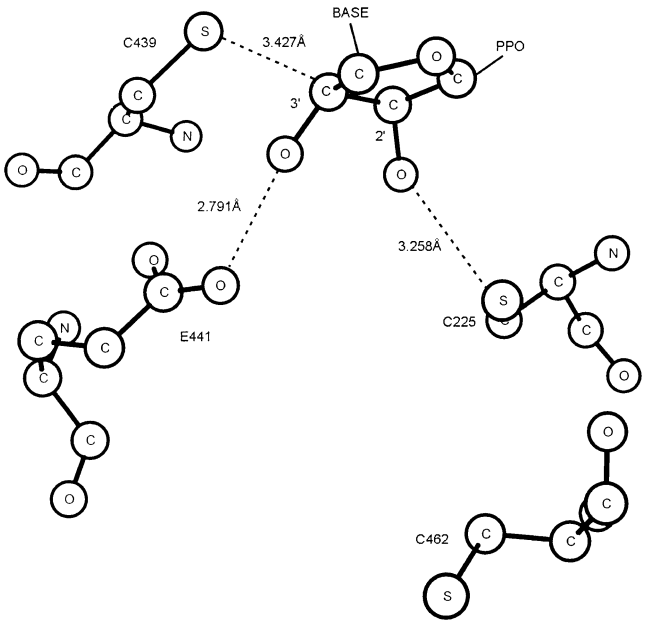

Figure 1. Active site of ribonucleotide reductase with the bound substrate.

protein.[2−4] It is a $\alpha_2\beta_2$ tetramer, constituted by two catalytically inactive homodimers.[24] The α_2 dimmer (R1 subunit) has a molecular weight of 171 kDa; the β_2 dimmer (R2 subunit) has a molecular weight of 87 kDa and (in Class I RNR) it possesses a stable tyrosil radical adjacent to a diiron cluster.[25,26] The tyrosil radical is originally formed in the R2 subunit, through hydrogen abstraction by the oxo-bridged diiron center, 35 Å away from the active site. The radical is transferred from Tyr122 near the diiron complex, to Cys439 at the active site in R1, through a chain of hydrogen-bonded residues.[27] The crystallographic structure of this enzyme with the bound substrate is shown in Figure 1.[28] Five conserved residues, namely three cysteines (C225, C439, and C462), one glutamate (E441) and one asparagine (N437) have been established as necessary for catalysis.[29,30]

FMCDP is an inhibitor of RNR that possesses potent chemotherapeutic efficacy against leukemia and solid tumors. The toxicity was initially thought to result from the ability of its triphosphates to function as DNA chain terminators in the DNA polymerase catalyzed elongation reaction.[11−14] However, because FMCDP can function as an inhibitor of RNR, it potentates the effect of the chain terminators by minimizing the competition for their incorporation into the DNA. FMCDP inhibits both R1 and R2 subunits of RNR, by destroying the essential tyrosil radical in R2 and alkylating the active site in R1.[10,31−33] Electron Paramagnetic Resonance (EPR) studies have determined that the loss of the tyrosil radical is accompanied by the formation of a new, substrate-derived radical.[10,33] Radiolabeling studies have suggested that this process involves addition of an active site residue to the substrate. Although attempts to isolate the alkylated amino acid have been unsuccessful, mutagenesis experiments with site-directed mutants of R1 have indicated that E441 should be the alkylated residue. Only C439 was not definitively excluded as the alkylated residue, because the C439S mutant is inactive, because C439 is the residue that initiates the catalytic reaction, after receiving the radical generated in R2. Analysis of the reaction products revealed that 1.5 equiv of inhibitor suffices to completely inactivate the enzyme, accompanied by the release of 1.5 equiv of fluoride and 0.5 equiv of cytosine. A new chromophore with a λ_{max} of 334 nm appears during inactivation. The existence of external reducing agents did not prevent inhibition, but it prevented chromophore formation. On the basis of these results,[32] and considering earlier mechanistic results with other 2′-substituted nucleotide analogues,[34−39] we have tried to explore theoretically all relevant mechanistic pathways, using Density Functional Theory, and arrived to a new mechanistic proposal coherent with the available experimental results and with the theoretical data.

The article is organized as follows: in section II, a brief description of the methods employed in this work is made, as well as their virtues and limitations. The proposed mechanisms are analyzed in section III, and compared with the available experimental data. The conclusions of this work are collected in section IV.

II. Methods

All calculations were performed using Density Functional Theory, with the Gaussian98 suite of programs,[40] at the unrestricted Becke3LYP level of theory.[41−43] In geometry optimizations and frequency analysis the 6-31G(d) basis set was used. The zero-point energies were calculated with the same theoretical level. It is well-known that larger basis sets give very small additional corrections to the geometries, and their use is hence considered unnecessary from a computational view.[18,44,45] The larger 6-311++G (3df, 3pd) basis set was used to calculate the energy of the optimized geometries. This basis

(24) Reichard, P. *Science* **1993**, *260*, 1773.
(25) Hammersten, E.; Reichard, P.; Saluste, E. *J. Biol. Chem.* **1950**, *183*, 105.
(26) Reichard, P.; Estborn, B. *J. Biol. Chem.* **1951**, *188*, 839.
(27) Siegbahn, P. E. M.; Eriksson, L.; Himo, F.; Pavlov, M. *J. Phys. Chem. B.* **1998**, *102*, 10 622.
(28) Eriksson, M.; Uhlin, U.; Ramaswamy, S.; Ekberg, M.; Regnstrom, K.; Sjöberg, B. -M.; Eklund, H. *Structure (London)* **1997**, *5*, 1077.
(29) Stubbe, J.; Ge, J.; Yee, C. *Trends in Biochem. Sciences* **2001**, *26*, 2, 93−99.
(30) Kasrayan, A.; Persson, A.; Sahlin, M.; Sjöberg, B.-M. *J. Biol. Chem.* **2002**, *277*, 5749.
(31) Sunkara, P.; Lippert, B.; Snyder, R.; Jarvi, T.; Farr, R. *Proc. Am. Assoc. Cancer Res.* **1998**, *29*, 324.
(32) van der Donk, W.; Yu, G.; Silva, D.; Stubbe, J.; McCarthy, J.; Jarvi, E.; Matthews, D.; Resvick, R.; Wagner, E. *Biochemistry* **1996**, *35*, 8381.
(33) van der Donk, W.; Gerfen, G.; Stubbe, J. *J. Am. Chem. Soc.* **1998**, *120*, 4252.
(34) Thelander, L.; Larsson, B. *J. Biol. Chem.* **1976**, *5*, 1398.
(35) Stubbe, J.; Kozarich, J. *J. Am. Chem. Soc.* **1980**, *102*, 2505.
(36) Stubbe, J.; Kozarich, J. *J. Biol. Chem.* **1980**, *12*, 5511.
(37) Sjöberg, B.-M.; Gräslund, A.; Eckstein, F. *J. Biol. Chem.* **1983**, *13*, 8060.
(38) Ator, M.; Salowe, S.; Stubbe, J.; Emptage, M.; Robins, M. *J. Am. Chem. Soc.* **1984**, *106*, 1886.
(39) van der Donk, W.; Stubbe, J.; Gerfen, G.; Bellew, B.; Griffin, R. *J. Am. Chem. Soc.* **1995**, *117*, 8908.
(40) Frisch, M. J.; Trucks, G. W.; Schlegel, H. B.; Scuseria, G. E.; Robb, M. A.; Cheeseman, J. R.; Zakrzewski, V. G.; Montgomery, J. A., Jr.; Stratmann, R. E.; Burant, J. C.; Dapprich, S.; Millam, J. M.; Daniels, A. D.; Kudin, K. N.; Strain, M. C.; Farkas, O.; Tomasi, J.; Barone, V.; Cossi, M.; Cammi, R.; Mennucci, B.; Pomelli, C.; Adamo, C.; Clifford, S.; Ochterski, J.; Petersson, G. A.; Ayala, P. Y.; Cui, Q.; Morokuma, K.; Malick, D. K.; Rabuck, A. D.; Raghavachari, K.; Foresman, J. B.; Cioslowski, J.; Ortiz, J. V.; Stefanov, B. B.; Liu, G.; Liashenko, A.; Piskorz, P.; Komaromi, I.; Gomperts, R.; Martin, R. L.; Fox, D. J.; Keith, T.; Al-Laham, M. A.; Peng, C. Y.; Nanayakkara, A.; Gonzalez, C.; Challacombe, M.; Gill, P. M. W.; Johnson, B. G.; Chen, W.; Wong, M. W.; Andres, J. L.; Head-Gordon, M.; Replogle, E. S.; Pople, J. A. *Gaussian 98*, revision A.9; Gaussian, Inc.: Pittsburgh, PA, 1998.
(41) Becke, A. D. *J. Chem. Phys. I* **1993**, *98*, 5648.
(42) Lee, C.; Yang, W.; Parr, R. J. *Phys. Rev. B* **1998**, *37*, 785.
(43) Hertwig, R. W.; Koch, W. *J. Comput. Chem.* **1995**, *16*, 576.
(44) Siegbahn, P. *J. Am. Chem. Soc.* **1998**, *120*, 8417.
(45) Forrester, J.; Frisch, A. In *Exploring Chemistry with Electronic Structure Methods*; Gaussian, Inc.; Pittsburgh, 1996; pp 64 and 157.

set is very close to saturation in the present system. The calculations were performed as follows: first, the geometry of the reactants and products of each mechanistic step were optimized. Those geometries were used to generate a guess for the transition state. Then, the transition state was located. Internal reaction coordinate calculations, followed by further tighter optimizations, were performed to determine which minima were connected to each transition state. Usually, these minima corresponded to the minima first determined. The structures of reactants and products discussed in this paper are the ones resulting from the internal reaction coordinate calculations. Frequency analyses were performed at each stationary point on the potential energy surface. The number of imaginary frequencies identified the nature of the stationary points (either minima or transition states). A scaling factor of 0.9804 was used for the frequencies. Thermal and entropic effects, considered less exact, were calculated at physiological temperature and added to the calculated energies, but analyzed separately.

The hydrogen-bonded complexes illustrated in this work have a very large number of minima. The particular structures discussed here were the ones that most closely reproduced the geometry of the active site. So, they are not necessarily the absolute minima for the complexes.

According to previous studies on active sites in proteins, the introduction of a dielectric continuum in the calculations with an empirical dielectric constant of 4 gives good agreement with experimental results, and accounts for the average effect of both the protein and the buried water molecules.[27,44,46,47] As our system contains charged species, it is important to evaluate the solvent effects. Moreover, some of the mechanisms studied here (namely the S_N2 reactions) are known to be solvent sensitive. Coherently, the energies were calculated under the influence of a dielectric continuum. To this purpose, we have used a Polarized Continuum Model, called C-PCM, as implemented in Gaussian98.[40] The continuum is modeled as a conductor, instead of a dielectric. This simplifies the electrostatic computations, and corrections are made a posteriori for dielectric behavior.

In open-shell systems, spin contamination is a frequent problem. It is well-known that DFT methods are quite robust to spin contamination, and in the calculations presented here, the expectation value for S^2 never reached a value of 0.78, before annihilation. After annihilation, the expectation value for S^2 never exceeded 0.7501. The Atomic spin density distributions were calculated with a Mulliken population analysis,[48] using the larger basis sets.

In the calculations methylthiol molecules modeled the cysteines. A formate molecule modeled the active site glutamate. The substrate analogues were modeled without the base and the diphosphate. The adequacy of these models was demonstrated in earlier works.[44,49] All explored mechanisms are discussed in the next section. The more favorable ones are described with more detail.

(46) Fernandes, P. A.; Eriksson, L. A.; Ramos, M. J., submitted for publication.
(47) Blomberg, M. R. A.; Siegbahn, P. E. M.; Babcock, G. T. *J. Am. Chem. Soc.* **1998**, *120*, 8812.
(48) Mulliken, R. S. *J. Chem. Phys.* **1955**, *23*, 1833.
(49) Himo, F.; Eriksson, L. A.; Catalytic Reactions of Radical Enzymes. In *Theoretical Biochemistry—Processes and Properties of Biological Systems*; Eriksson, L. A., Ed.; Elsevier Science: New York, 2001.

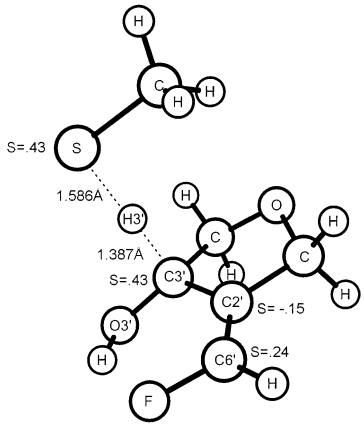

Figure 2. Transition state for the abstraction of the H3′ atom by C439. Distances in Å, spin densities in a.u.

III. Results and Discussion

Scheme 1 illustrates the several possible pathways for inhibition here explored. These reflect the most appealing mechanisms from a chemical point of view.

The first mechanistic step (the activation of the inhibitor) is uncontroversial, as it is well supported by experimental evidences.[33] It is common to all pathways, and a prerequisite for the subsequent steps. It is similar to the reaction with the natural substrate, and corresponds to the abstraction of the H3′ atom by C439. The transition state is depicted in Figure 2 (only atoms relevant for the mechanism are numbered). The spin density is almost evenly shared between the sulfur atom of C439 and the C3′ of the inhibitor, although the C6′ retains considerable spin density also. At the reactants the spin density was localized at the sulfur atom of C439 (0.97 au), and in the products the spin becomes localized at the C3′ (0.52 au) and at the C6′ (0.64 au). Coherently, the C2′ has a spin density of −0.24 au.

The C2′−C3′ and C2′−C6′ bond lengths (see Figure 2 for atom numbering) also change considerably in this reaction. In the reactants, the C2′−C3′ bond length corresponds to 1.524 Å and the C2′−C6′ bond length corresponds to 1.324 Å, typical distances for a single and a double bond, respectively. In the products, the C2′−C3′ bond shortens to 1.386 Å and the C2′−C6′ bond increases to 1.376 Å, distances intermediate between the characteristic CC single bond and double bonds, a consequence of the delocalization of the double bond character. The activation free energy is calculated to be 9.8 kcal/mol and the free energy of reaction −7.7 kcal/mol. Thermal and entropic contributions are of 4.2 kcal/mol in the barrier and 1.4 kcal/mol in the reaction free energy. It is interesting to compare those energies with the ones obtained for the same mechanistic step with the natural substrate, at the same theoretical level. According to previous calculations (not shown here) the activation free energy for abstraction of the H3′ atom from cytosine diphosphate (CDP) is 12.3 kcal/mol, close to the 9.8 kcal/mol obtained with FMCDP. However, activation of CDP is endothermic by 6.9 kcal/mol, in striking contrast to the value of −7.7 kcal/mol obtained for FMCDP. This reflects the much greater stability of the radical generated from FMCDP, which spin density becomes almost evenly delocalized through the C3′ and the C6′ atoms, and not mainly confined to the C3′ atom, as in the case of CDP.

In an earlier experimental work, it was determined that the kinetics of inhibition was multiphasic, with several pathways

Scheme 1. Explored Inhibition Pathways. All Energies in kcal/mol

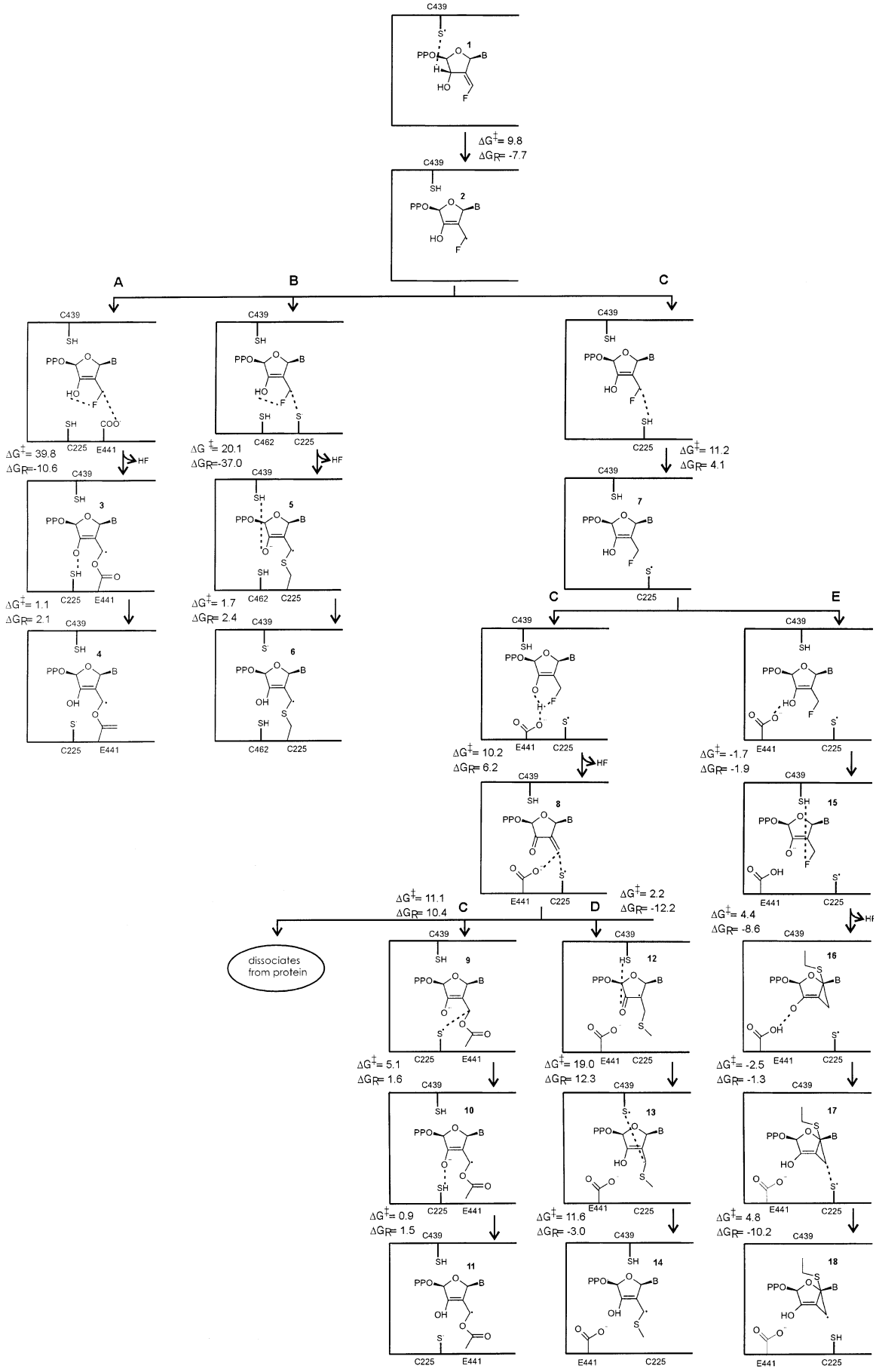

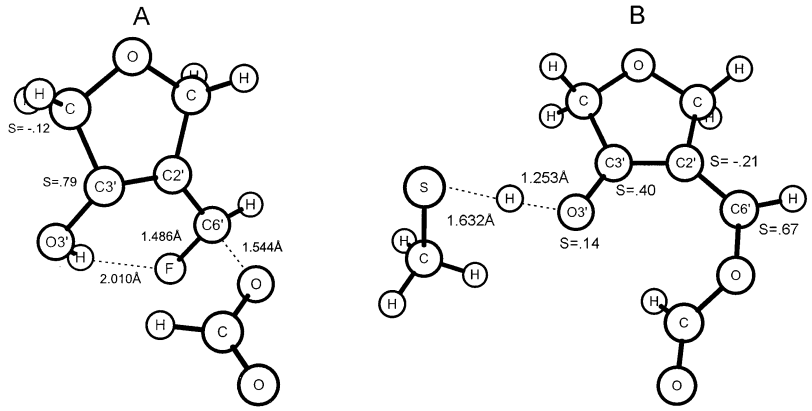

Figure 3. (A) Transition state for the alkylation of intermediate 2 by E441. (B) Transition state for the proton transfer to the 3′ oxygen of the inhibitor. Spin densities in a.u., distances in Å.

competing, and such conditions precluded the determination of accurate kinetic parameters.[32] So, it is not possible to estimate an upper level for the activation energies, to seek for agreement with experiments. However, this does not present a problem as, in the major catalytic pathway, the first step is the rate-determining step, known to occur as schematized in Figure 2. Activation of the substrate leads to several possible pathways.

IIIa. Pathway A. The first and obvious choice corresponds to the addition of E441 to the inhibitor. According to pathway **A** in Scheme 1, the oxygen of E441 adds to the C6′, in an S_N2 reaction, and elimination of fluoride occurs concerted with alkylation, resulting in the intermediate **3**. Subsequent protonation of the O3′ would lead to the final product **4**. Several donors for such proton could be postulated. As the C3′ has a sp^2 hybridization the oxygen can be accessed from both faces of the inhibitor, and all active site cysteines (C225, C429, C462) can function as proton donors. Such a very simple mechanism would be in line with the earlier proposal that E441 is the alkylating residue, based on the inadequacy of the E441Q mutant to alkylate the inhibitor.[10,32,33]

The transition state for the addition of glutamate is depicted in Figure 3A.

The transition state can be considered as a late transition state, as the C6′-O bond is almost formed (1.544 Å at the transition state and 1.408 Å in the products). The C6′-F bond is only slightly distended (1.486 Å at the transition state and 1.397 Å in the reactants), and the fluorine atom is still very distant from the 3′ hydroxyl hydrogen (note that IRC calculations, starting from the transition state of Figure 2, show that the fluorine atom abstracts the hydroxyl hydrogen after the addition of the glutamate, and leaves the active site as HF). Main changes in the spin distribution correspond to a shift of spin density from the C3′ to the O3′, due to the establishment of a keto−enolate equilibrium in the products. The activation free energy for this step amounts to 39.8 kcal/mol and the reaction free energy to −10.6 kcal/mol. Thermal and entropic contributions amount to 3.2 kcal/mol in the barrier and 1.6 kcal/mol in the reaction energy. This barrier clearly seems too high, but the inexistence of experimental kinetic data precludes neglect of this pathway solely based on the activation energy. So, we proceeded to the next step, the protonation of the O3′ by a cysteine, to obtain the final product **4**. The transition state for such reaction is depicted in Figure 3B above.

Spin density shifts from the O3′ to the C3′, when going from the reactants to the products. The change is caused by the shift in the keto−enolate equilibrium toward the enolic form, when the oxygen is protonated. The activation free energy for this step corresponds to 1.1 kcal/mol and the reaction free energy to 2.1 kcal/mol. Thermal and entropic terms contribute negligibly to the barrier and the reaction free energy.

The high barriers obtained for this mechanism strongly suggest one of the two following possibilities: the alkylating residue is not the glutamate, and the final product of inhibition should be other than **4**, or another mechanism for glutamate addition, with lower activation energy, must be found. To test the first hypothesis, another pathway leading to another inhibition product must be considered.

IIIb. Pathway B. The natural choice is to replace the glutamate by an anionic cysteine, whose thiolate is adequate to perform a nucleophile attack to the C6′ of the inhibitor (pathway B, Scheme 1). Subsequent protonation of the O3′ would lead to the final product. It was noticed before that FMCDP was resistant to attack by thiolates with pH up to 9,[32] and it was anticipated that the activation of the inhibitor must be a prerequisite for such attack. The anionic cysteine can be either C225 or C462. Both of them lie in the α-face of the inhibitor and C225 is making a hydrogen bond with the 2′ hydroxyl group in the X-ray crystallographic structure. C462 is a bit more distance, but it can easily approach the inhibitor, since those cysteines form a sulfur bond in the normal catalytic pathway. Mutagenesis experiments with the C225S and C462S mutants failed to reveal a substantial decrease in the alkylation of R1 relative to the wt-RNR (0.70, 0.75 and 0.92 equiv. of radiolabel per equiv of R1, respectively[32]). Although this suggests that C225 and C462 are not directly involved in the process of alkylation, it does not preclude such hypothesis. Both cysteines are in very close proximity, and when one is engineered to a serine, the other can replace its role in the inhibition mechanism. Only the double mutant C225/462S could reveal unambiguous conclusions about the direct involvement of these cysteines.

The transition state for the addition of a thiolate to the C6′ of the substrate is shown in Figure 4A. That corresponds also to an S_N2 reaction, with hydrogen fluoride release concerted with the addition of the thiolate, as observed previously in pathway A.

At the transition state the spin density is mostly localized at the C6′, although some spin density is delocalized to the sulfur atom. The spin density in the reactants is shared between the C3′ and C6′ atoms (0.52 u.a. and 0.64 u.a., respectively). In the products the spin density is mostly localized at the C6′ (0.60

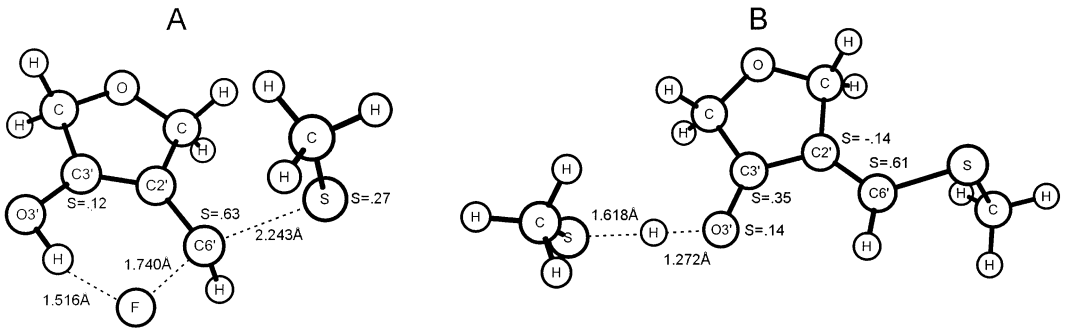

Figure 4. (A) Transition state for the addition of thiolate to the activated inhibitor 2. (B) Transition state for the proton transfer from C439 to the O3′ of intermediate 5. Spin densities in a.u., distances in Å.

au) but the C3′ and the O3′ still retain some spin density (0.28 au and 0.16 au, respectively). Internal reaction coordinate calculations revealed a similar behavior as with the E441 addition, i.e., that the fluorine atom abstracts a proton from the 3′ hydroxyl, being eliminated as HF, and then dissociating in solution producing fluoride, as observed experimentally, and the intermediate **5**. Note that at the transition state the fluoride ion is already making a strong hydrogen bond with the 3′hydroxyl hydrogen. The activation free energy for this step corresponds to 20.1 kcal/mol and the reaction free energy to −37.0 kcal/mol. Thermal and entropic contributions amount to 1.4 kcal/mol in the barrier and 1.0 kcal/mol in the reaction free energy. The process is strongly exothermic, and the barrier for the inverse process amounts to 57.1 kcal/mol. Such a barrier fully justifies the irreversibility of the inactivation, as observed experimentally. Finally, to obtain the product of inactivation **6**, the anionic O3′ must abstract a proton to return to its normal protonation state. The transition state for such proton transfer is depicted in Figure 4B above (we have considered C439 as the protonating agent in the calculations. The spin pattern does not change very much is this step. There is a shift in the spin density from the O3′ to the C3′ and C6′ atoms, when going from the reactants to the products. The change is again caused by the shift in the keto−enolate equilibrium, toward the enolic form when the oxygen is protonated. The activation free energy for this step corresponds to 1.7 kcal/mol and the reaction free energy to 2.4 kcal/mol. Thermal and entropic contributions amount to 0.6 kcal/mol in the barrier and 0.4 kcal/mol in the reaction free energy. So, protonation is a very fast step.

Although this mechanism is to be preferred over pathway A, it does not seem to be able to explain all experimental results. Namely, why alkylation is so strongly decreased in the E441Q mutant, as this residue does not play a determinant role in the above mechanism. And even though we could not exclude the possibility that the role of E441 might be to better bind the substrate, we decided to explore other possible pathways that eventually accommodated better the existing experimental data.

IIIc. Pathway C. Another piece of experimental evidence that is mechanistically informative is that the EPR spectrum of the transient radical is composed by an ∼1:1 mixture of a doublet and a triplet signal when (*E*)-[6′-^{2}H]-FMCDP is incubated with the wt-RNR. An explanation proposed by Stubbe and co-workers[10] resorts to an H-atom transfer equilibrium between the C6′ and one of the cysteines, namely C225. The cysteine transfers an H atom to the C6′, and unrestricted rotation around the C2′−C6′ bond can lead the cysteine to either re-abstract a hydrogen atom or a deuterium atom, resulting in a

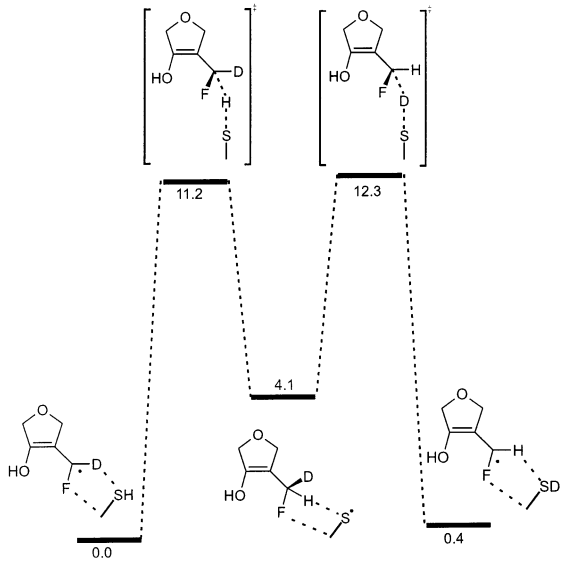

Figure 5. H atom transfer between activated FMCDP 2 and a cysteine. Note that in the present example the cysteine abstracts a deuterium atom, but unrestricted rotation about the C2′−C6′ bond can lead the cysteine to re-abstract the deuterium or a hydrogen atom instead.

mixture of ∼1:1 of deuterated and nondeuterated FMCDP. Although such mechanism sounds appealing from a chemical point of view, we performed theoretical calculations on that equilibrium to investigate its feasibility, before starting to explore new pathways derived from it. To accommodate the experimental spectrum two conditions must be met: the reactants and products must be close in energy and the barrier for the transfer cannot be too large as this would make the equilibrium too slow to be relevant. Figure 5 shows the results obtained. As can be seen, the difference in free energy corresponds to only 0.4 kcal/mol and the free energy barriers for the limiting steps in the two directions (11.2 and 11.9 kcal/mol) are not high enough to preclude such mechanism. The barrier for the first H-atom transfer is even faster than addition of the thiolate, especially if we keep in mind that the pK_a for the thiol group of a proteic cysteine is ca. 8−9, and so the proportion of the thiolate form corresponds only to 1−10% at physiological pH.

So, we are led to the conclusion that Stubbe's explanation does take us to 2′-fluoromethanedCDP intermediate **7**, from which alternative pathways may be derived. Fluoride elimination can be achieved by an intramolecular rearrangement. The fluorine atom can abstract the 3′ hydroxyl hydrogen and be eliminated as HF. The reactive 2′-methylene-3′-ketodCDP intermediate **8** obtained from this reaction is also an irreversible

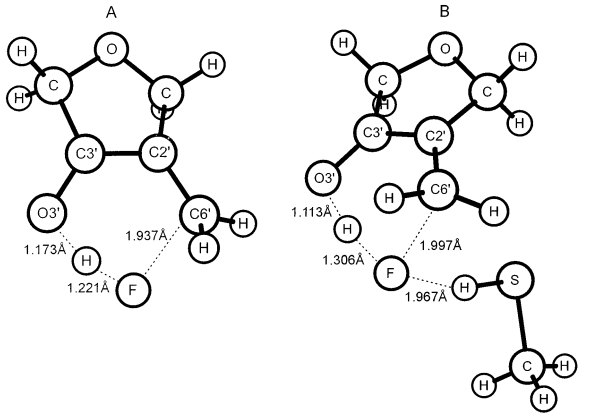

Figure 6. (A) Transition state for intramolecular fluoride elimination. (B) Transition state for the proton transfer from C439 to the O3′ of intermediate 5. Distances in Å.

inhibitor of RNR.[50−52] It was demonstrated that this compound decomposes in solution, losing base and phosphate, and generates a furanone derivative (4-methyl-2-methylene-3 (2*H*)-furanone) that is highly reactive to nucleophilic attack. Subsequently, the furanone performs unspecific alkylation of R1, resulting in enzyme inactivation.[50] Similar chemistry was also observed with other 2′-substituted nucleotide analogues.[53,54] The present case has however an important difference, the 2′-methylene-3′-ketodCDP intermediate **8** is generated inside the active site. Accordingly, it can react further with the active site residues, or dissociate into solution, lose the base and the diphosphate (explaining the slow release of the base and phosphate into solution observed experimentally with FMCDP) and convert into the reactive furanone species, which will be trapped by the enzyme.[10,32] To explore such alternative pathways, we began by investigating the formation of the intermediate **8**. This exercise led us into two situations, which have not been depicted in Scheme 1 basically because their activations energies were too high. They will be, however, described next, and depicted in Figure 6. The transition state for the intramolecular rearrangement is depicted in Figure 6A.

At the transition state the C6′-F bond is very elongated, and making a short, strong hydrogen bond with the 3′ hydroxyl hydrogen, which is already leaving the O3′ atom. The free energy barrier for such rearrangement corresponds to 20.8 kcal/mol and the reaction free energy to −13.2 kcal/mol. Thermal and entropic contributions amount to 1.0 kcal/mol for the barrier and −0.5 kcal/mol for the reaction free energy. The activation energy is clearly too high for this process to be competitive with the thiolate addition. So, another mechanism should exist to generate the intermediate **8**, if it is to be formed. The first hypothesis considered was to use another of the cysteines to facilitate the fluorine release, by partial protonation of the fluoride. Such transition state is shown in Figure 6B.

The free energy barrier for the C225 assisted rearrangement amounts to 21.7 kcal/mol and the reaction free energy to −11.7 kcal/mol. Thermal and entropic contributions correspond to 1.4 kcal/mol in the barrier and −0.2 kcal/mol in the free energy of reaction. So, partial protonation of the fluorine with C225 does not lead to a decrease in the free energy barrier, as was desired. Instead, it rises by 1.0 kcal/mol, reflecting the fact that the cysteine stabilizes more the reactants than the transition state.

However, another residue that can catalyze fluoride elimination is E441. We started by trying to find a concerted transition state similar to the one of Figure 6B, with the carboxylate making a hydrogen bond with the leaving hydrogen, but the unfavorable interaction of the carboxylate with the fluoride and with the O3′ atom precluded such geometry. Instead, we found that a stepwise mechanism for the fluoride elimination would be much more favorable. In the first step, the glutamate would abstract a proton from the 3′ hydroxyl group. Then, it must break the hydrogen bonding network with the O3′, and make a hydrogen bond with the fluorine atom. This turned out to be the limiting step for the catalysis. After such complex has been formed, the glutamic acid protonates the fluoride, that leaves the active site as HF. Figure 7 illustrates this mechanism, which leads to the formation of intermediate **8** in Scheme 1.

Note that in this reaction we have modeled glutamate as acetate to better model the hydrogen bonds with the aliphatic hydrogens. The starting structure **7a** has the proton already transferred to the glutamate. The transition state and the energetics for this very fast step are not presented here because the same reaction was modeled with a larger model to explore pathway E (see Figure 10(A) and corresponding energetics). Structure **7b** is a true transition state, linking two minima with a different hydrogen-bonding network. The glutamic acid, initially strongly hydrogen-bonded to the O3′, forms two long hydrogen bonds with the O3′ and with the fluorine atoms. In intermediate **7c**, the acidic hydrogen makes a strong hydrogen bond with the fluorine atom. The C6′-F bond is now elongated from 1.450 Å in the reactants to 1.577 Å in the products. The second step consists of the protonation of the fluorine by the glutamic acid. At the transition state, the C6′−F bond is very elongated, even though the OH bond of the acidic hydrogen is only slightly elongated, reflecting the facility to eliminate fluoride by this mechanism. In the product **7e** fluoride is eliminated as HF and the intermediate **8** is generated.

The first step (reorganization of the hydrogen bonding network) is the rate limiting with an activation free energy of 10.2 kcal/mol, and a reaction free energy of 6.2 kcal/mol. Thermal and entropic contributions are −0.2 kcal/mol for the barrier and −0.6 kcal/mol for the reaction free energy. The protonation of the fluorine and elimination of HF constitutes a fast step, with a very small free energy barrier of 1.5 kcal/mol. The reaction free energy corresponds to −19.5 kcal/mol. Thermal and entropic contributions represent −0.2 kcal/mol of the barrier and −3.4 kcal/mol of the reaction free energy. We can now conclude that the formation of the intermediate **8** is only feasible if catalyzed by E441, thus explaining the inability of the E441Q mutant to alkylate quantitatively the substrate. This suggests that E441 is indeed important for inhibition, not by adding to the inhibitor, but instead by catalyzing a rate-limiting step. The intermediate **8** formed in this step is highly activated toward nucleophile addition, and according to the mechanism proposed by Stubbe and co-workers (major pathway), would add covalently to an active site residue, inhibiting irreversibly the enzyme. In that mechanistic proposal[32] the next step would be the addition of E441 to the intermediate **8**.

(50) Baker, C.; Banzon, J.; Bollinger, J.; Stubbe, J.; Samano, V.; Robins, J.; Lippert, B.; Jarvi, R.; Resvick, R. *J. Med. Chem.* **1991**, *34*, 1879.
(51) Robins, J.; Samano, V.; Zhang, W.; Balzarini, J.; De Clercq, E.; Borchardt, R.; Lee, Y.; Yuan, C.-S. *J. Med. Chem.* **1992**, *35*, 2283.
(52) Samano, V.; Robins, J. *J. Org. Chem.* **1991**, *56*, 7108.
(53) Stubbe, J. *Adv. Enzymol*. **1989**, *63*, 349.
(54) Ator, M.; Stubbe, J. *Biochemistry* **1985**, *24*, 7214.

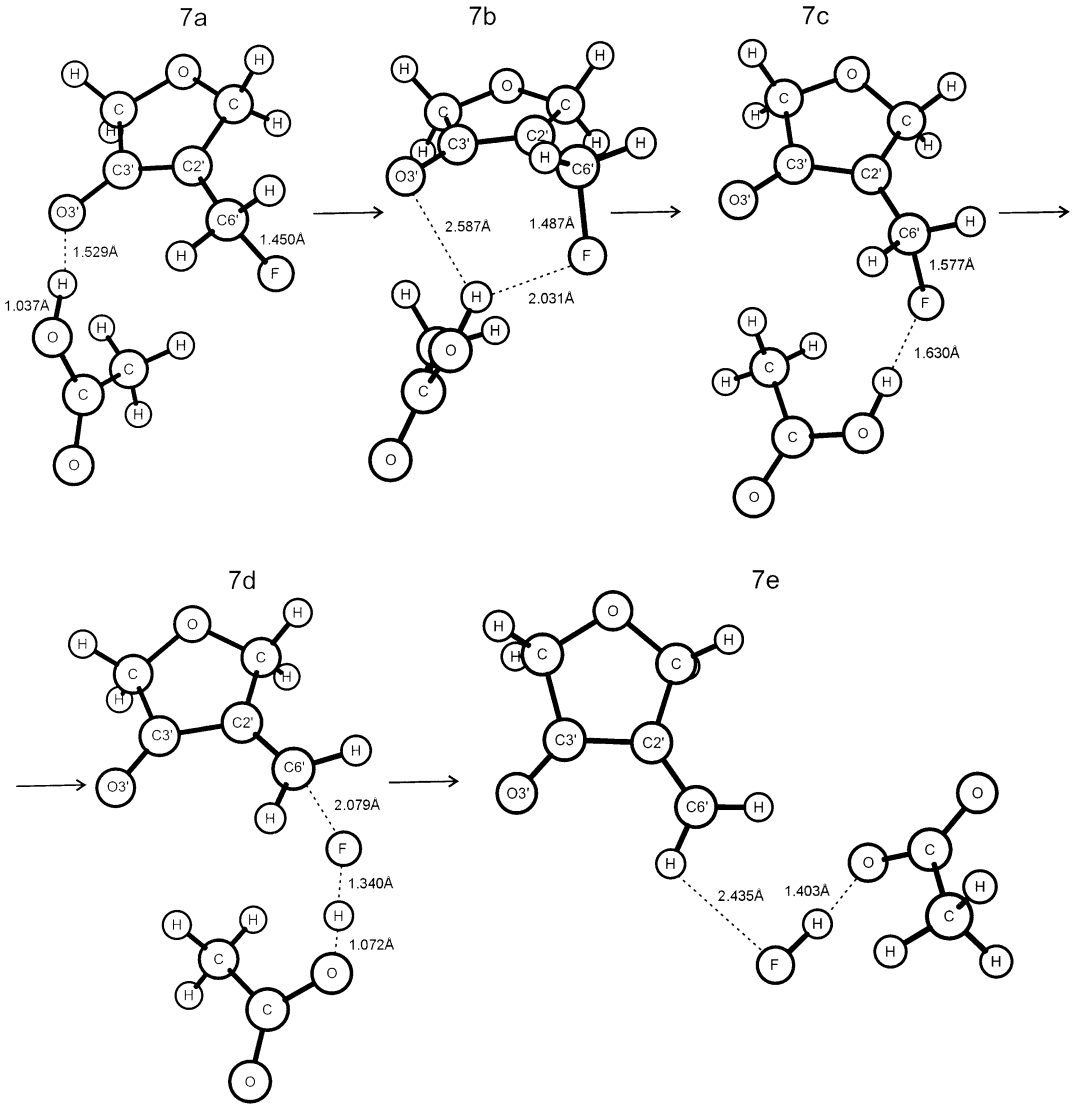

Figure 7. Pathway for stepwise elimination of HF, catalyzed by E441. All distances in Å.

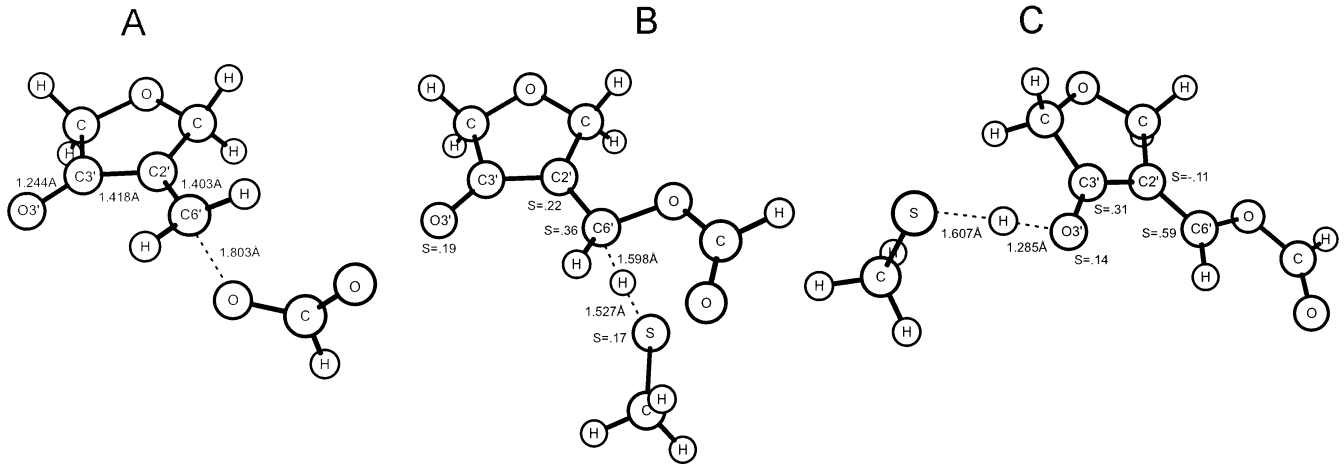

Figure 8. (A) Transition State for the addition of E441 to the 2′-methylene-3′-ketodCDP intermediate 8. (B) Transition state for hydrogen atom abstraction from the C6′ of the intermediate 9. (C)Transition State for proton transfer to O3′. All distances in Å, spin densities in a.u..

Another hypothesis in line with the previous results (pathway **A)** is that addition to the intermediate **8** could be done by an active site cysteine. To be on the safe side, we explored both pathways, starting from intermediate **8**. To begin with, addition of E441 will be explored (continuation of pathway **C**, Scheme 1). The transition state for such reaction is represented in Figure 8A.

The keto−enolate equilibrium is shifted toward the enolic

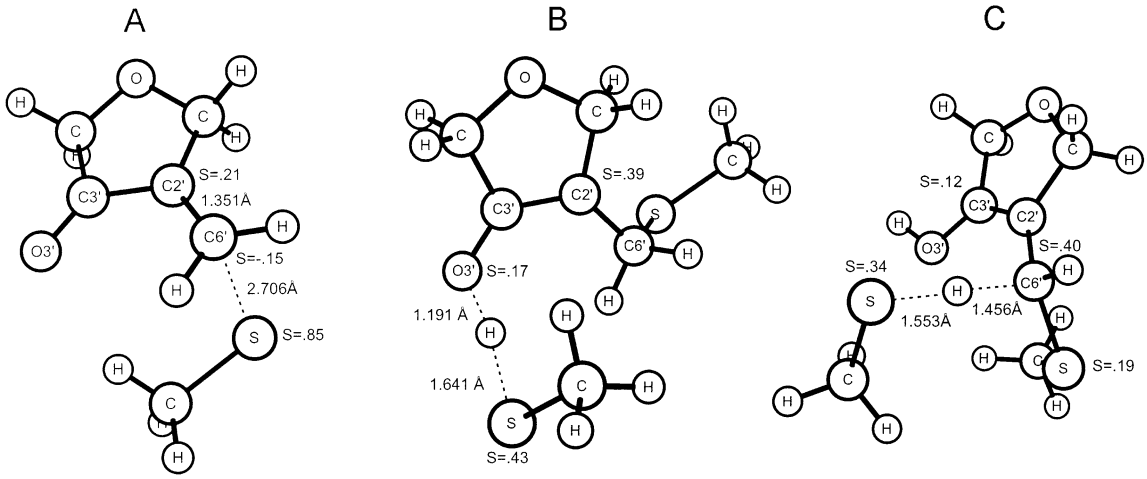

Figure 9. (A) Transition State for cysteine addition to the intermediate 8. (B) Transition State for hydrogen atom transfer to the intermediate 12. (C) Transition State for proton transfer to O3′. All distances in Å, spin densities in a.u..

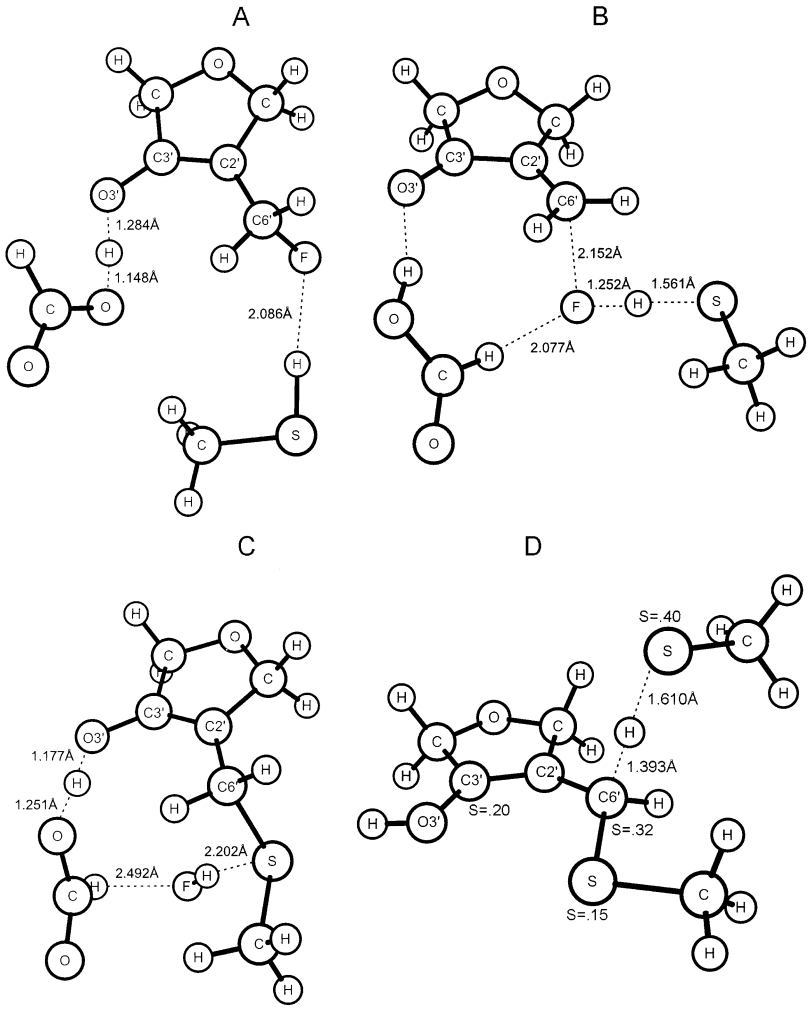

Figure 10. (A) Transition state for proton transfer from the 3′hydroxyl to E441. (B) Transition state for protonation of fluorine followed by cysteine addition to C6′. (C) Transition state for proton from E441 to the 3′ oxygen. (D) Transition state for hydrogen atom abstraction from C6′. All distances in Å, spin densities in a.u..

form when E441 adds to the intermediate **8**, as can be seen by the changes in geometry when going from the reactant to the product (increase in the C3′−O3′ and the C2′−C6′ bond lengths, and decrease in the C2′−C3′ bond length). The free energy of activation corresponds to 11.1 kcal/mol and the reaction free energy to 10.4 kcal/mol. Thermal and entropic contributions increase the barrier and the reaction free energy by 1.8 and 1.6 kcal/mol, respectively. So, the equilibrium clearly favors the intermediate **8**, and not the alkylated product **9**. However, this unfavorable equilibrium can eventually be overcome if the subsequent steps are fast and thermodynamically favorable. The next step in this mechanism is the abstraction of a hydrogen

atom from the C6′ by the radical cysteine, with a subsequent protonation of the O3′. The transition state for hydrogen abstraction is depicted in Figure 8B above.

Note that this pathway implies that E441 can add to the C2′ and C225 can protonate the O3′ atom. Looking at the geometry of the active site (Figure 1) it can be seen that the residues must move considerably, and change their relative positions to undergo the reaction. That seems difficult in a rigid enzyme as RNR. So, we propose that if this pathway is to occur, the first hydrogen atom transfer (Figure 7) should be performed by C439. Coherently, the hydrogen transfer from C6′ to O3′ would be performed by C439 also. This gas-phase equivalent pathway seems more viable in the active site of the enzyme. Moreover, C439 is better positioned to reach both the C6′ and the C3′ atoms, because the substrate must move in that direction when E441 adds to C6′. In reactant **9** the spin density distribution is localized at the C2′ atom (0.42 au) and at the sulfur of C439 (0.47 au), due to the charge transfer from the thiolate and the consequent keto−enolate equilibrium. In product **10**, after proton transfer, the spin density shifts to the C6′ and the O3′ atoms (0.55 au and 0.18 a.u, respectively); the spin density is now almost null in the sulfur atom and only 0.09 au in the C2′ atom. The free energy barrier for this reaction is 5.1 kcal/mol and the reaction free energy 1.6 kcal/mol. Thermal and entropic contributions represent 1.8 kcal/mol in the barrier and 0.8 kcal/mol in the reaction energy. The next step corresponds to C439 transferring the proton to the O3′ atom, thus generating the final product **11**. The transition state is shown in Figure 8C above.

The spin distribution shifts from C2′ and O3′ to C3′, after protonation. The C6′ atom retains almost the same spin density as in the transition sate. The free energy barrier is also very small, amounting only to 0.9 kcal/mol. The reaction free energy corresponds to 1.5 kcal/mol. Thermal and entropic contributions represent 0.5 kcal/mol in the barrier and 0.1 kcal/mol in the reaction energy. This mechanistic step is also not thermodynamically favorable, and the final product **11** lies 13.5 kcal/mol above the intermediate **8**. Should this unfavorable thermodynamic equilibrium be the main reason the radical produced by the inhibition does not result from E441 addition?

IIId. Pathway D. To find an answer for that question we turned back to intermediate **8**, and considered the possibility of the addition of a radical cysteine (C439 or C225, depending in which one has initially protonated the activated inhibitor **2**) to the C6′ of intermediate **8**. Such addition will probably lead to a pathway **D** ending on a product similar to the one resultant from pathway **B**.

The transition state for the addition of the radical cysteine is illustrated in Figure 9A. This is an early transition state, with the sulfur atom at a distance of 2.706 Å from the C6′.

The spin density is mainly located at the sulfur atom initially, and is transferred to the C2′ and slightly to the O3′ on the products. Geometry changes follow the same trends, with an increase in the C3′−O3′ and C2′−C6′ bond lengths. We verified that geometry and spin density distribution change just slightly from the reactants to the transition state, and change extensively from the transition state to the products, as is typical of an early transition state. This reaction has a low activation free energy, as is expected from the similarity between the reactants and the transition state, corresponding to 2.2 kcal/mol. The reaction free energy corresponds to −12.2 kcal/mol. Thermal and entropic contributions amount to 1.8 kcal/mol in the barrier and 2.9 kcal/mol in the reaction free energy.

So, the barrier for cysteine addition to the intermediate **8** is much lower than the barrier to E441 addition. Moreover, the reaction is exothermic by −12.2 kcal/mol, in contrast to the endothermicity of 10.4 kcal/mol to the glutamate addition. This clearly explains why E441 does not ads to intermediate **8**. The reason is that the competitive addition of a cysteine is kinetically and thermodynamically much more favorable. However, it was shown that such ketyl radical **12** cannot be the final inhibition product, as g_{iso} values and isotropic coupling constants for that radical do not mach the ones obtained by incubation of wt-RNR with FMCDP, within experimental accuracy.[33] This opens up two trains of thought. The ketyl radical **12** either rearranges to the allylic radical **14** as previously obtained from pathway **B** or it dissociates from the active site faster than cysteine addition. To elucidate which is the case, we tried several pathways that led from the ketyl radical **12** to the allylic radical **14**. The most favorable corresponds to a hydrogen atom transfer to the O3′, by the remaining active-site cysteines, followed by abstraction of a hydrogen atom from the C6′, by the radical cysteine generated in the earlier step. The transition state for the first is exhibited in Figure 9B above.

In this reaction, the spin distribution is transferred from the C2′ to the cysteine sulfur. At the transition state the spin density is almost evenly distributed between the C2′ and the cysteine sulfur; in the reactant **12** the spin density is mainly located at the C2′ (0.72 au) and at the O3′ (0.26 au). In product **13**, the spin density is located at the sulfur of the cysteine (0.97 au). Geometric changes are related to the elongation of the C3′−O3′ bond and the shortening of the C2′−C3′ bond, due to the keto to enol conversion. The free energy barrier for this reaction corresponds to 19.0 kcal/mol and the reaction free energy to 12.3 kcal/mol. Thermal and entropic contributions amount to 3.2 kcal/mol in the barrier and 3.0 kcal/mol in the reaction free energy. The subsequent and final step of this pathway corresponds to the abstraction of a hydrogen bound to C6′ by the radical cysteine resultant from the earlier step. The transition state for that reaction is depicted in Figure 9C above.

In this mechanistic step the spin density is transferred from the cysteine sulfur to the C6′ and C3′. At the transition state, the spin is almost evenly shared by the cysteine sulfur and the C6′. In the reactants the spin density is mainly confined to the sulfur (0.90 au). In the products the spin density is shared between the C3′ (0.44 au) and the C6′ (0.63 au). The double bond character of the C2′−C3′ is now delocalized also to the C6′, which leads to a shortening of the C2′−C6′ bond and an increase in the C2′−C3′ bond length. The activation free energy for this reaction corresponds to 11.6 kcal/mol and the reaction free energy to −3.0 kcal/mol. Thermal and entropic contributions amount to 2.3 kcal/mol in the barrier and 0.7 kcal/mol in the free energy of reaction.

Although these two steps are not energetically prohibitive, the ketyl radical **12** should be stable enough to be detected by EPR spectroscopy, and we know this is not the case.[33] Once formed, it has a free energy barrier of 19.0 kcal/mol to proceed forward and a free energy barrier of 14.4 kcal/mol to proceed in the reverse direction. As far as we can see, considering the geometry and the residues of the active site, there is no other viable pathway to transform the ketyl radical **12** in the allylic

radical **14**. The obvious conclusion is that dissociation from protein is faster than cysteine addition. So, we conclude that the earlier proposed minor pathway (the solution pathway) results from pathway **C**, i.e., after the intermediate **8** is formed (catalyzed by E441) it dissociates from the active site, losing base and phosphate and originating the unsaturated 4-methyl-2-methylene-3 (2*H*)-furanone, that subsequently performs unspecific addition to the active site.[10,32,50]

IIIe. Pathway E. However, the major inhibition pathway remains elusive. In the conversion of the natural substrate, elimination of the 2′hydroxyl group is achieved by deprotonation of the 3′ hydroxyl and protonation of the 2′hydroxyl group by C225, with a water molecule leaving the ring. So, we considered that elimination of fluoride and subsequent cysteine addition could be achieved by a mechanism similar to the natural catalytic pathway. Besides this hypothesis, we could not see any other viable pathway that accommodates the experimental data. We tried first to find a concerted pathway for hydrogen abstraction and fluoride protonation, but our efforts proved unsuccessful. Then, we considered performing the reaction stepwise; the first step would be a 3′ hydroxyl proton abstraction, by E441, followed by fluoride protonation. The transition state for the first step is illustrated in Figure 10(A).

Such very fast proton transfer has a very small electronic barrier that disappears after adding the zero-point energy. Considering thermal and entropic corrections (−0.8 kcal/mol), it is located 1.7 kcal/mol below the reactants. The reaction free energy corresponds to −1.9 kcal/mol, including −1.8 kcal/mol from the thermal and entropic contributions. The keto−enolate equilibrium in product **15** leads to a shortening of the 3′CO bond length (from 1.321 to 1.281 Å) and a subsequent elongation of the 6′C−F bond length (from 1.430 to 1.465 Å), facilitating subsequent protonation. Afterward, a cysteine (most probably C439, considering that C225 performs the earlier hydrogen atom transfer to the C6′, generating intermediate **7**) protonates the fluorine atom, mimicking the natural substrate pathway.[29] The transition state for the protonation is exhibited in Figure 10B. It must be noticed that extensive Internal Reaction Coordinate calculations demonstrate that product **16** connected to the transition state of Figure 10B includes cysteine addition to C6′ atom of the inhibitor. So, fluoride elimination and cysteine addition occur in the same mechanistic step.

At the transition state, the 6′C−F bond is very elongated, and the proton is already almost abstracted. Fluoride eliminates as HF, as in previous cases. The sulfur atom is still distant from C6′, although it will add to it from this transition state. Spontaneous addition of thiolate was predictable, as preliminary calculations (not reported here) have shown that thiolate adds spontaneously, without barrier, to intermediate **8**. The structure of the transition state is quite similar to intermediate **8**, which means that it should be a low energy structure. This is confirmed by the small activation free energy for this step, which corresponds to 4.4 kcal/mol. The reaction free energy amounts to −8.6 kcal/mol. Thermal and entropic contributions represent −0.9 and 1.7 kcal/mol to the barrier and reaction energy, respectively. This is by far the most favorable pathway for inhibition and undoubtfully corresponds to the elusive major pathway for inhibition. It is interesting to note that the enzyme indeed eliminates HF through the same mechanism by which it eliminates the 2′ hydroxyl in the normal catalytic pathway.[29] To fully confirm that this is the case, two experimental evidences must be met: first, the E441 residue must assist this step, since the E441Q mutant exhibits a much smaller degree of active-site alkylation. Second, there must be a viable pathway to convert the intermediate **16** to the final product **18**. To investigate the first we tried to perform the fluoride elimination without abstracting the 3′hydroxyl hydrogen. Such reaction is very improbable, because the reactant is neutral and the transition state would have a charge separation (a thiolate and a carbocation), which should be highly energetic. After trying several different initial structures, we observed that such transition state does not exist in the present potential energy surface. When the cysteine partially protonates the fluorine atom to facilitate fluoride elimination, and the C6′−F bong elongates**,** the fluoride abstracts a proton from the 3′hydroxyl group instead, and not from the cysteine, leading always to the transition state presented in Figure 6B. So, we confirm that E441 is indeed essential for the proposed mechanism, in full agreement with mutagenesis experiments.[32]

To convert **16** to the final product **18**, we propose a two-step mechanism. First, E441 protonates the O3′, that returns to the correct protonation state generating the intermediate **17**; afterward, the radical cysteine C225 abstracts a proton from C6′, generating the final product **18**. Both steps must be fast and thermodynamically favorable. The transition state for the proton transfer is depicted in Figure 10C.

This transition state corresponds to the inverse process shown in Figure 10A, including now hydrogen bonding network with the leaving HF molecule. Accordingly, it is also a fast step with a very small electronic barrier that disappears after adding the zero-point energy, and becomes located 2.5 kcal/mol below the reactants. The reaction free energy corresponds to −1.3 kcal/mol. Thermal and entropic corrections amount to 0.6 kcal/mol in both the barrier and the reaction energy. In product **17** the keto−enol equilibrium shifts toward the enolic form, leading to an increase in the C3′−O3′ bond length (from 1.284 to 1.324 Å) and a subsequent decrease of the C2′−C3′ bond length (from 1.377 to 1.354 Å). Afterward, abstraction of a hydrogen atom from C6′ atom by the same cysteine leads to the final stable radical **18**. C225 is perfectly positioned to carry out the reaction, and it is predictable that the cysteine is able to abstract the hydrogen, as it corresponds to a reaction similar to the activation of the substrate. Moreover, it is already in the radical form. The transition state for hydrogen abstraction is shown in Figure 10D. During this reaction the spin density distribution is transferred from the cysteine sulfur to the C6′ and C3′ atoms. Spin densities for sulfur range from 0.90 au in the reactants to 0.0 au in the products, for C6′ they range from 0.0 au in the reactants to 0.54 au in the products and for C3′ from 0.0 au in the reactants to 0.43 au in the products. The sulfur of the bound cysteine also has considerable spin density at the end of the reaction (0.17 au). In the products, the C2′ atom also retains a final spin density of −0.19 au. Geometric changes are small and mainly caused by the greater delocalization of the π electrons, mostly localized at the C2′−C3′ bond in the reactants and delocalized to the C6′ and the sulfur atom of the bound cysteine in the products. Consequently, the C2′−C3′ bond length increases from 1.338 to 1.375 Å, and the C2′−C6′ and C6′−S bond lengths decrease from 1.494 to 1.396 Å and from 1.837 to 1.756 Å, respectively. The activation free energy for this

reaction corresponds to 4.8 kcal/mol and the reaction energy to −10.2 kcal/mol. Thermal and entropic contributions represent 4.2 kcal/mol in the barrier and 0.3 kcal/mol in the reaction free energy.

We conclude that both mechanistic steps have low activation barriers and are thermodynamically favorable (the first one is almost thermoneutral). Therefore, intermediate **16** rearranges quantitatively to the final inhibition product **18**. So, the major inhibition pathway is determined, and corresponds to addition of a cysteine to the inhibitor via protonation of fluorine, mimicking the normal catalytic pathway.

IV. Conclusions

We have performed a detailed study of the potential energy surface of a model of the active site of RNR with the bound FMCDP inhibitor. Several inhibition pathways were explored resorting to theoretical calculations. The obtained results were then compared with available experimental data.

It was established that the major inhibition pathway evolves protonation of fluoride by a cysteine with subsequent elimination of fluoride and addition of the cysteine to the inhibitor. Earlier mechanistic proposals preferred addition of a glutamate to the inhibitor, instead of a cysteine. Such preference was corroborated by the large decrease in alkylation of the inhibitor with the E441Q mutant. However, theoretical results show that addition of E441 is neither kinetically competitive nor thermodynamically viable. Moreover, it was shown here that the E441 residue has a fundamental role in the addition of the cysteine to the inhibitor, thus explaining mutagenesis results. It is interesting to note that the mechanism for fluoride elimination and subsequent thiolate addition mimics the mechanism for 2′-hydroxyl elimination in the substrate catalytic pathway, reinforcing the credibility of the theoretical proposal, and showing that studies with inhibitors can be very informative about the capabilities of the enzyme machinery in the conversion of the natural substrate. The minor inhibition pathway (the solution pathway) was also identified as resulting from the generation of the 2′-methylene-3′-ketodCDP intermediate. It was predicted before[10,32] that this intermediate would be formed and afterward leave the active site, lose base and fluoride (detected in solution), rearrange to a furanone derivative, and alkylate nonspecifically the enzyme. However, in that mechanistic proposal, the major pathway results from addition of E441 to intermediate **8**, which we demonstrate not to be the case. The results obtained here show also that E441 catalyzes both minor and major inhibition pathways.

Acknowledgment. Fundação para a Ciência e Tecnologia (Project POCTI/35736/99, Portugal) and the National Foundation for Cancer Research (NFCR-U.S.A.) are gratefully acknowledged for financial support.

Supporting Information Available: Molecular coordinates for all stationary points. This material is available free of charge via the Internet at http://pubs.acs.org.

JA0208613